Simulation of alternative process schemes for hydrofluoric and phosphoric acid stream treatment and nutrient recovery

Kelly Ohanessian, Cristian Barca*, Audrey Soric, Jean-Henry Ferrasse, Olivier Boutin

Aix Marseille Univ, CNRS, Centrale Marseille, M2P2, Marseille, France

*Corresponding author: cristian.barca@univ-amu.fr

Abstract

Hydrofluoric and phosphoric acid streams produced by the microelectronic industry usually present high flow and high contents of phosphorus, nitrogen, fluorine, and organic carbon. This study aims at evaluating the efficiency and suitability of alternative process schemes for the treatment and valorization of hydrofluoric and phosphoric acid streams. A comparative approach is followed, based on the simulation of different process schemes, each involving several steps of physicochemical and biological treatments. The main objectives are to compare (i) the treatment efficiency, (ii) the consumption of chemical reagents, and (iii) the recovery of high-value by-products (*e.g.* calcium fluoride, struvite, and hydroxyapatite), and hence to identify the most suitable process scheme. Furthermore, this study contributes to the development of chemical precipitation and bioconversion models that can be applied for further simulation studies on wastewater treatment processes. The results indicate that the use of calcium hydroxide ($Ca(OH_2)$) as the only source of Ca^{2+} and OH^- ions for the precipitation steps is a promising way to reduce the total consumption of chemical reagents while recovering high purity (> 98%) calcium fluoride and struvite. Moreover, the use of a membrane aerated biofilm reactor after the precipitation steps may further decrease organic carbon and nitrogen contents below 125 g $COD.m^{-3}$ and 30 g $N.m^{-3}$, thus allowing effluent discharge to natural waters. Overall, this study gives useful information for the development of innovative treatment

processes and it provides crucial data for the selection of the most promising alternative schemes.

Keywords: Water treatment; Process coupling; Simulation; Microelectronic wastewater; Nutrient recovery.

1. Introduction

Nowadays, rapid expansion of electronic equipment in the world contributes to negative effects on the environment, such as pollution in manufacturing plants, shortage of raw materials, increase in energy consumption, accumulation of electronic wastes, and production of a large amount of aqueous and gaseous effluents [1]. Microelectronic industries produce five main different types of wastewater streams: (i) acids and bases streams, (ii) hydrofluoric and phosphoric acids stream (HPA), (iii) ammonia and organic matter streams, (iv) chemical mechanical polishing (CMP) stream, and (v) CMP copper stream. These wastewater streams have high contents of various pollutants such as phosphorus (P), nitrogen (N), fluorine (F), heavy metals, suspended solids, strong oxidants (*e.g.* H_2O_2), and organic matter [2–5]. Because of their complex composition, they often require different steps of treatment to reach the standards for discharge (*e.g.* chemical precipitation, chemical oxidation, filtration, adsorption and/or ionic exchange). Therefore, the development of alternative process schemes to improve the performance and to reduce the total costs of their treatment is receiving an increasing attention [4,6–9].

Among the different streams from microelectronic industry, HPA stream usually presents low pH (≤ 2), high flow (10-100 $m^3.h^{-1}$), and high contents of F (75-1,336 g $F.m^{-3}$), P (5-388 g PO_4-$P.m^{-3}$), ammonia (80-250 g NH_4-$N.m^{-3}$), and acetic acid (221-444 g $COD.m^{-3}$) [4,5,10,11]. Nowadays, the conventional treatment process for HPA stream consists of two consecutives steps of chemical precipitation to remove F, P, and N. First, precipitation of calcium fluoride (CaF_2) is obtained at pH 4 by the addition of calcium chloride ($CaCl_2$) and sodium hydroxide

(NaOH) to increase the pH from 1-2 to 4. Then, the precipitation of P and N under the form of struvite ($NH_4MgPO_4.6H_2O$) is obtained at pH 7-9 by the addition of magnesium chloride ($MgCl_2$) and NaOH [5]. The recovery of CaF_2 and struvite from microelectronic wastewater is very interesting because they can be valorized as secondary raw materials for the production of hydrofluoric acid and for the manufacture of fertilizers, respectively [12,13]. However, these precipitation steps require the consumption of a high amount of chemicals. In addition, after struvite precipitation, the effluent usually requires a supplementary biological treatment to further reduce its N and organic carbon contents before the discharge to natural waters. The high flow of HPA streams may require large volumes for conventional biological reactors, and therefore the investment and operating costs may be too expensive. In addition, the discharge of these effluents to municipal wastewater treatment plants (WWTP) may lead to further costs and technical problems such as dilution of the organic load. Therefore, the development of alternative process schemes may represent a viable solution to reduce the consumption of chemicals and to produce effluents that can be directly rejected to natural waters, thus improving performance, and reducing the total cost of the full treatment process.

Several strategies have been proposed in the literature to improve performance of industrial wastewater treatment, such as enhanced thermochemical, physicochemical, and biological processes, or the combination of these processes [14–17]. However, to the best of our knowledge, there is a lack of studies in the literature that have dealt with the development of alternative treatment processes for HPA stream. This study aims at evaluating the suitability of alternative process schemes for the treatment and valorisation of HPA stream. A simulation approach is used as a tool of analysis to evaluate: (i) the treatment efficiency, (ii) the consumption of chemical reagents, and (iii) the recovery of high value by-products (*e.g.* calcium fluoride, struvite, hydroxyapatite). First, models for each unit operation (chemical precipitation and bioconversion steps) are build using experimental data from the literature, including

solubility and thermodynamic data for chemical species, and conversion yields and kinetic data for the bioconversion steps. Second, several process schemes, based on the coupling of different unit operations, are identified and built in the software ProSimPlus®, and their treatment performances are simulated. Finally, the results of simulations are compared to identify the most promising alternative schemes.

The novelty and importance of this paper are highlighted by the following points:

(i) The first comparative study based on the simulation of alternative process schemes for the treatment and valorisation of HPA stream. This simulation approach presents the advantage of obtaining a rapid prediction of treatment performances without building prototypes or carrying out real experiments.

(ii) The development of modules to simulate phosphate precipitation and bioconversion processes. Indeed, phosphate species and bioconversion modules are often not available in the most common commercial softwares. The modules developed in this study can be further adapted and used to simulate phosphate recovery and/or bioconversion processes for different types of wastewaters (*e.g.* effluents from food, painting, textile, pharmaceutical industries).

2. Materials and methods

2.1. HPA stream composition

Table 1 summarizes the concentrations of fluorine (F), phosphate (PO_4-P), ammonia nitrogen (NH_4-N), acetic acid (expressed as chemical oxygen demand, COD), and sulphate (SO_4-S) of HPA effluents reported in the literature. As shown in Table 1, F, PO_4-P, NH_4-N, and COD range between 75-1,336 g $F.m^{-3}$, 5-388 g PO_4-$P.m^{-3}$, 80-250 g NH_4-$N.m^{-3}$, and 221-444 g $COD.m^{-3}$, respectively, thus indicating that chemical composition of HPA stream may vary according to the different production sites and manufacturing processes. Table 1 also summarizes the concentrations of chemical species in HPA stream that are considered for simulation in this study, which are in agreement with the data from James and Gerbino [10]. According to the

literature [5,18,19], HPA stream flows vary between a large range of values depending on the size of the different production sites (10 - 100 $m^3.h^{-1}$). A value of 100 $m^3.h^{-1}$ is considered in this study to simulate a big-size production site.

Table 1. HPA stream composition data from the literature and data used for simulation (N.A. = not available).

Compound	Huang et al., [4][a]	Warmadewanthi and Liu, [11][b]	Ryu et al., [5][c]	James and Gerbino, [10][d]	Chemical species and concentrations used for simulation in this study
F ($gF.m^{-3}$)	1,280 ± 56	1,336	75-799	950	1,000 g $HF.m^{-3}$
P (gPO_4-$P.m^{-3}$)	201 ± 3,4	256,3	5-388	388	400 g $H_3PO_4.m^{-3}$
N (gNH_4-$N.m^{-3}$)	131 ± 5,1	212,7	80 - 250	180	350 g $NH_4OH.m^{-3}$
COD ($gO_2.m^{-3}$)	N.A.	N.A.	221-444	321	300 g $CH_3COOH.m^{-3}$
S (g SO_4-$S.m^{-3}$)	N.A.	N.A.	N.A.	356	1,000 g $H_2SO_4.m^{-3}$

a. Average values ± standard deviation

b. Average values

c. Range min-max values

d. Average values

2.2. Simulation software

ProSimPlus® software (Labège, France) is used for the simulations. This software allows to simulate different unit operations with a large choice of chemical components, thermodynamic models, and process modules that are available in the database. ProSimPlus® provides to the user calculated data on flow rates and chemical concentrations, as well as thermodynamic data of the main outcomes (*e.g.* temperature, pressure, enthalpy, entropy, physical state). However, this software has some shortcomings, as some chemical compounds and process modules are

missing from the database (*e.g.* phosphate species and bioconversion modules). To solve this problem, the user can add chemical compounds in the software database, can interact with a platform for special thermodynamic models, and can create windows script modules coded in Visual Basic language and user modules coded in Fortran language.

2.3. Development of chemical precipitation modules

The crystallization module that is proposed by ProSimPlus® is used to simulate the precipitation steps. The electrolytic model Sour Water is chosen as thermodynamic model for the simulations. This model describes the thermodynamic equilibrium between electrolytes in aqueous solutions and it can be applied for temperatures between 0 to 200 °C and pressures between 0.1 MPa to 5 MPa. Sour Water is based on the calculation of activity molecule coefficients using the Pitzer model, and on the calculation of enthalpy values by the Helgeson-Kirkham-Flowers model (HKF model) [20]. It can predict the precipitation of chemical compounds according to the temperature, the pressure, the pH, and the chemical composition of aqueous solutions. Among the chemical compounds that are addressed in this study, calcium fluoride (CaF_2) is already implemented in the software database, whereas struvite, hydroxyapatite (HAP), and fluorapatite (FAP) are missing. Therefore, struvite, HAP, and FAP are defined in the software database by adding for each compound molecular and thermodynamic data taken from the literature. The data added to the software database are chemical formula, molar mass, physical state at 25 °C in aqueous solution, solid enthalpy formation ($\Delta H°s$), solid Gibbs energy formation ($\Delta G°s$), solid molar volume at 25 °C (Vms), and correlations between solid specific heat (Cp^S) and temperature (Table 2).

Table 2. Molecular and thermodynamic data for calcium fluoride, struvite, hydroxyapatite (HAP), and fluorapatite (FAP).

Name	Formula	Molar mass ($g.mol^{-1}$)	$\Delta H°s$ ($kJ.mol^{-1}$)	$\Delta G°s$ ($kJ.mol^{-1}$)	Vm_S ($cm^3.mol^{-1}$)	Cp^S ($J.mol^{-1}.K^{-1}$)
Calcium fluoride	CaF_2	78.075	-1,226 [d]	-1,113.5 [d]	-	Equation 1[d]
Struvite	$NH_4MgPO_4,6H_2O$	245.4	-3,681.9[a]	-3,051.1[a]	144.54[b]	346,3[c]
Hydroxyapatite	$Ca_5(PO_4)_3OH$	502.32	-6,669.26[a]	-6,301.5[a]	158.99[b]	Equation 2
Fluorapatite	$Ca_5(PO_4)_3F$	504.3	-6,840[a]	-6,452[a]	158.43[b]	Equation 3

a. From La Iglesia, [21]

b. From Chichagov et al., [22]

c. Cp^S at 25 °C [23]

d. ProSimPlus® database

The correlation between Cp^S ($J.mol^{-1}.K^{-1}$) and temperature T (K) for CaF_2 is already implemented in the software database (Equation 1), whereas the correlations for HAP and FAP are added to the database by considering literature data [24], as shown in Equations 2 and 3, respectively.

$$C_p^S(CaF_2) = -262.49 + 140.52\,T \quad (1)$$

$$C_p^S(HAP) = 387.76 + 0.11856\,T + 1{,}811.2\,T^{-0.5} - \frac{1{,}270{,}3000}{T^2} \quad (2)$$

$$C_p^S(FAP) = 754.33 - 0.030255\,T - 6{,}200.5\,T^{-0.5} - \frac{90{,}8380}{T^2} \quad (3)$$

However, no Cp^S correlation is found for struvite in the literature. Therefore, the Kopp's rule method (Equation 4) is used to determine the Cp^S value at 25 °C, where C_i is a constant associated with each element in the compound ($J.mol^{-1}.K^{-1}$), N_i is the number of occurrences of the element in the compound, and Misc represents elements that do not have a specific constant

(*e.g.* P). According to Hurst and Harrison [23], the constants are 18.74, 7.56, 13.42, 22.68, and 26.63 $J.mol^{-1}.K^{-1}$ for N, H, O, Mg, and Misc, respectively.

$$C_p^S = (\sum_{i=1}^{n} C_i \times N_i) + C_{Misc} \times N_{Misc} \quad (4)$$

In order to describe the dissociation of phosphoric acid in solution, PO_4^{3-}, HPO_4^{2-}, and $H_2PO_4^-$ ions are defined in the software database before simulations. For each ion, the Helgeson coefficients (a_1, a_2, a_3, a_4, c_1, and c_2), the Born constant, the molar mass, the charge, and thermodynamic data as Gibbs energy formation ($\Delta G°_h$) and entropy at infinite dilution ($S°_h$) were added to the database (Table 3, adapted from Shock and Helgeson [25]).

Table 3. Helgeson coefficients, Born constant and thermodynamic data of phosphate ions *[25]*.

Ionic species	**Helgeson coefficients**						**Born constant**	**$\Delta G°_h$ (cal.mol^{-1})**	**$S°_h$ (cal.mol^{-1}.K^{-1})**
	a_1	**a_2**	**a_3**	**a_4**	**c_1**	**c_2**			
$H_2PO_4^-$	0.64875	805.95	2.5823	-31,122	14.0435	-44,605	130,030	-270,140	21.6
HPO_4^{2-}	0.36315	108.57	5.3233	-28,239	2.7357	-149,103	333,630	-260,310	-8
PO_4^{3-}	-0.05259	-906.54	9.3131	-24,042	-9.475	-264,397	561,140	-243,500	-53

The correlations between solubility product K_S and temperature T (K) for struvite, HAP, and FAP are also determined by using experimental data from the literature, as shown by Equations (5), (6), and (7), respectively [26,27].

$$\log Ks\,(Struvite) = 6 \times 10^{-5}\,T^3 - 0.0624\,T^2 + 20.279\,T - 2{,}219 \quad (5)$$

$$\log Ks\,(HAP) = {}^{-8{,}219.41}/_{T} - 1.6657 - 0.098215\,T \quad (6)$$

$$\log Ks\,(FAP) = 0.0036\,T^2 - 2.3024\,T + 228.76 \quad (7)$$

Finally, molecular and thermodynamic data of other chemical compounds missing from the database, including NaH_2PO_4, Na_2HPO_4, Na_3PO_4, $(NH_4)_2HPO_4$, $NH_4H_2PO_4$ $(NH_4)_3PO_4$, $Ca_3(PO_4)_2$, $Ca(H_2PO_4)_2$, $CaHPO_4$, $CaHPO_4.2H_2O$, $Mg(H_2PO_4)_2$, $MgHPO_4$, $Mg_3(PO_4)_2$, $Mg_5(PO_4)_3OH$, $MgSO_4$, $MgSO_4.H_2O$, $MgSO_4.2H_2O$, $MgSO_4.4H_2O$, $MgSO_4.5H_2O$, $MgSO_4.6H_2O$, $MgSO_4.7H_2O$, and $MgSO_4.11H_2O$, are added to the database. This is done to consider all possible compounds that can precipitate.

2.4 Development of bioconversion modules: Aerated activated sludge reactor (CSTR)

The conventional activated sludge process is considered to simulate aerobic biodegradation of acetic acid and ammonia nitrogen uptake by heterotrophic bacteria. The activated sludge reactor is modeled according to a continuous stirred tank reactor (CSTR), and it is written in a windows script module. The activated sludge model n 1 (ASM1 model) is employed to describe the biodegradation process [28], and the values used for μ_{max}, Ks, Y and R_N are 0.25 h^{-1}, 15 $g_{COD}.m^{-3}$, 0.67 $g_X.g_{COD}^{-1}$, and 0.07 $g_N.g_X^{-1}$, respectively. These values are commonly used for easily biodegradable organic substrate [29]. The following assumptions are proposed: steady state conditions are reached, biomass is composed of heterotrophic bacteria, and oxygen is not limiting the aerobic respiration. The hydraulic retention time (HRT) and biomass concentration are set to 4 h and 2500 $g.m^{-3}$ based on literature data [30], thus leading to a reactor volume of 400 m^3 according to the flow rate of the effluent (100 $m^3.h^{-1}$).

2.5 Development of bioconversion modules: Membrane aerated biofilm reactor (MABR)

The membrane aerated biofilm reactor (MABR) is considered to simulate partial nitrification of ammonia nitrogen to nitrite and heterotrophic denitrification using acetic acid as carbon substrate [31]. These processes are usually carried out in different reactors because nitrification occurs under aerobic conditions while denitrification prevails in the absence of oxygen [32]. In addition, two bacterial populations are involved in the full treatment process: autotrophic

bacteria for the nitrification step and heterotrophic bacteria for the denitrification step. Differently from conventional activated sludge systems, the MABR allows to perform these two steps simultaneously in a single reactor. MABR modules are usually composed of a vertical cylindrical tank where dense polydimethylsiloxane hydrophobic hollow fibers are used as biofilm carriers and gas suppliers. The fibers are permeable to gas, thus allowing the transfer of oxygen to the biofilm. According to literature data, the number of fiber, the internal and outer diameter of the fibers, the length of the fibers, the reactor height and the ratio height to diameter of the reactor are set to 1210, 2 mm, 3 mm, 2 m, 2.1 m, and 5, respectively [33,34], thus giving a volume of 0.29 m^3 for each MABR module.

2.5.1 MABR biofilm model

MABR is modelled according to a three-layer diffusion model: (i) bulk liquid, (ii) boundary layer, and (iii) biofilm, as shown in Fig.1. The boundary layer induces dissolved compounds mass transfer resistance between bulk liquid and biofilm. Four components are considered: biomass as particulate compound, and ammonium, nitrite, and acetic acid as dissolved compounds. The biomass is composed of autotrophic nitrifying and heterotrophic denitrifying bacteria. The following assumptions are proposed: steady state conditions are reached, biofilm is at its maximum possible thickness, biofilm growth is balanced by cells detachment, oxygen is the limiting substrate in the case of aerobic bioconversions, and diffusion and bioconversion reactions both occurred inside the biofilm. The presence of suspended biomass in bulk liquid and boundary layers is neglected.

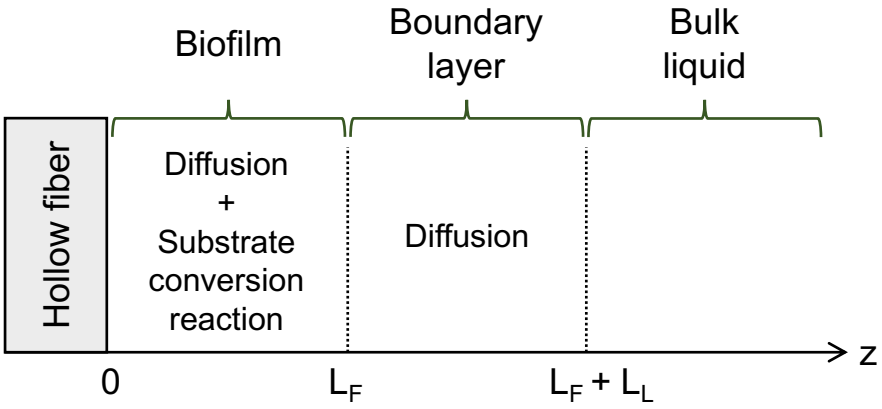

Fig. 1. Schematic presentation of the three-layer diffusion model for MABR.

The MABR biofilm model used in this study is based on the results of previous studies that have investigated oxygen transfer profiles inside MABR biofilms [31]. The model involves three different biofilm layers (Fig. 2). The first layer of aerobic autotrophic biomass grows at the surface of the membrane fibers (0-300 μm), where higher oxygen and lower acetic acid concentrations favor aerobic autotrophic rather than heterotrophic bacteria. The second layer of aerobic heterotrophic biomass grows on the surface of the autotrophic layer (300-500 μm from the fiber surface), where residual acetic acid and oxygen allows aerobic respiration. The third layer of anoxic heterotrophic biomass grows on the surface of the second biomass layer (500-2000 μm from the fiber surface), where lower oxygen and higher acetic acid concentrations allow heterotrophic denitrification.

Nitrite produced by the autotrophs is used as electron acceptor for heterotrophic denitrification, while CO_2 produced by heterotrophs is used as carbon source for autotroph growth [35]. Partial nitrification of ammonium to nitrite is operated by autotrophic ammonia oxidating bacteria. However, autotrophic nitrite oxidating bacteria can further oxidize nitrite to nitrate, thus increasing the oxygen consumption of the system [36]. In this study, the control of dissolved oxygen concentration is considered as the key strategy to obtain a stable partial nitrification.

Indeed, at low dissolved oxygen concentration, the rate of nitrite oxidation by autotrophic nitrite oxidating bacteria is lower than that of ammonium oxidation by autotrophic ammonia oxidating bacteria. Several studies in the literature confirm the key role played by dissolved oxygen on partial nitrification [37–39]. According to their findings, concentrations higher than 2.5 g $O_2.m^{-3}$ may favour a complete oxidation of ammonium to nitrate, whereas concentrations between 0.3 and 1.5 g $O_2.m^{-3}$ can inhibit autotrophic nitrite oxidating bacteria thus giving more stable partial nitrification. Therefore, 1 g $O_2.m^{-3}$ is set as optimum dissolved oxygen concentration for partial nitrification in this study.

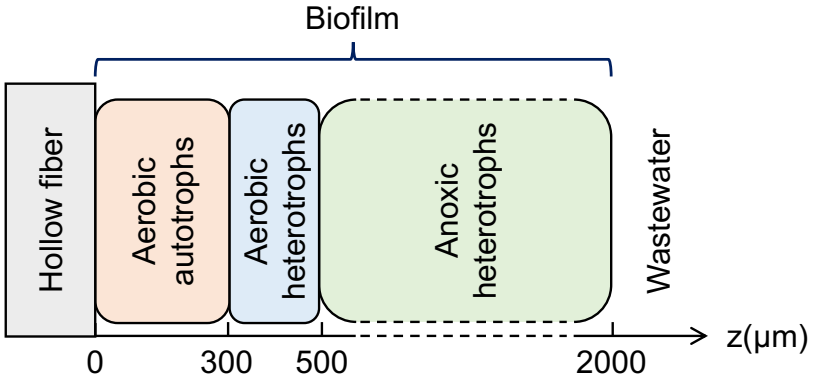

Fig. 2. Biofilm layer model for MABR.

2.5.2 Mass transfer in MABR biofilm

The Equations (8-10) are used for the mass balances of each dissolved compound in the liquid phase, in the boundary layer, and in the biofilm, respectively, as summarized in Fig. 1. C_{in}^S is the substrate concentration in the influent ($g.m^{-3}$), C_B^S is the substrate concentration in the bulk liquid ($g.m^{-3}$), j_F^S is the substrate flux ($g.m^{-2}.s^{-1}$), A_F is the total biofilm surface area (m^2), D_L^S is the diffusion coefficient of the substrate in the liquid (aqueous) phase ($m^2.s^{-1}$), D_F^S is the diffusion coefficient in the biofilm ($m^2.s^{-1}$), and r_S is the substrate conversion rate ($g.m^{-3}.s^{-1}$). For each substrate, the value of r_S is determined according to a Monod kinetic model matrix

(section 2.5.3 MABR bioconversion model). The following assumptions are proposed: the input flux and initial concentrations are known, the liquid phase is perfectly stirred, the output flux is equal to input flux, and the biofilm is flat and homogeneous.

$$Q\left(C_{in}^{S} - C_{B}^{S}\right) + j_{F}^{S} A_{F} = 0 \quad (8)$$

$$D_{L}^{S} \frac{d^2 C^S}{dz^2} = 0 \quad (9)$$

$$-D_{F}^{S} \frac{d^2 C^S}{dz^2} + r_S = 0 \quad (10)$$

For each substrate, D_F^S is estimated by the empirical correlation propose by Fan et al. [40] (Equation (11)), where X represents the density of the autotrophic and/or heterotrophic biofilm layer (g.m^{-3}). The value of X is estimated by the empirical correlation proposed by Hibiya et al. [41] (Equation (12)), where L_F is the thickness of the biofilm layer (m). The values of D_L^S are set to $2 \cdot 10^{-9}$, $1.2 \cdot 10^{-9}$, $1.7 \cdot 10^{-9}$, and $1.6 \cdot 10^{-9}$ m^2.s^{-1} for oxygen, acetic acid, ammonium, and nitrite diffusion in the liquid phase, respectively [31].

Commenté [FJh1]: LF est fixée à 2000 u mais es tec que tusais comment est calculée LL? Ou alors LL est calculée grace à V2 ?
Les valeurs sont ells compatibles ?

$$\frac{D_F^S}{D_L^S} = 1 - \frac{0.43 \cdot X^{0.92}}{11.19 + 0.27 \cdot X^{0.99}} \quad (11)$$

$$X = 2.5.10^4 + 1.5.10^5 \cdot exp\left({}^{-L_F \cdot 10^6}/_{175}\right) \quad (12)$$

Equations (13-16) are also considered to respect the following conditions: continuity of concentrations at the liquid/boundary layer interface (Equation (13)), continuity of concentrations and mass fluxes at the boundary layer/biofilm interface (Equation (14)), and no flux at the biofilm/support interface (Equation (15)). L_L is the boundary layer thickness (m), C_F^S is the substrate concentration at the biofilm/boundary layer interface (g.m^{-3}), and k_S is the substrate mass transfer coefficient (m.s^{-1}) calculated by Equation (16). Ammonium and acetic acid initial concentrations are known, and no flux of these compounds at the biofilm/support interface is considered.

$$C^S(z = L_L + L_F) = C_B^S \quad (13)$$

$$j_F^S = -D_F^S \frac{dC^S}{dz}|_{z=L_F} = -k_S(C_F^S - C_B^S) \quad (14)$$

$$-D_F^S \frac{dC^S}{dz}|_{z=0} = 0 \quad (15)$$

$$k_S = \frac{D_L^S}{L_F} \quad (16)$$

The heterotrophic biofilm layer growing on the surface of the autotrophic layer can induce a further mass transfer resistance for ammonium [42]. Therefore, the ammonium transfer coefficient k_{NH4} ($m.s^{-1}$) is calculated by Equation (17), where L_H is the thickness of the heterotrophic biofilm layer (m).

$$k_{NH4} = \frac{D_L^S D_F^S}{D_L^S L_H + D_F^S L_L} \quad (17)$$

The system of Equations (8-17) is solved as a second-order non-linear differential equation. The resolution is done using the 4th order Adams–Bashforth method initialized with the Runge–Kutta 4 method.

2.5.3 MABR bioconversion model

The Monod kinetic model is used to describe acetic acid as well as ammonium and nitrite bioconversion processes in the biofilm. The model matrix described by Dosta et al. [43] is used to determine the expression of the substrate conversion rates r_S ($g.m^{-3}.s^{-1}$). Moreover, the ammonium inhibition constant K_I of 271 $gNH_4\text{-}N.m^{-3}$ is used in the model to take into account the inhibitory effect of ammonium on ammonia oxidating bacteria [44]. Table 4 summarizes the conversion yields and kinetic parameters that are used for the bioconversion model.

Table 4. Kinetic parameters used to model biodegradation in MABR.

Parameter	Value	Reference
μ_{max}^{AOB} (d^{-1})	0.9	[45]
μ_{max}^{AA} (d^{-1})	0.25	[46]
μ_{max}^{H} (d^{-1})	1.5	[47]
$K_{NH4,AOB}$ ($g.m^{-3}$)	0.7	[45]
$K_{AA,A}$ ($g.m^{-3}$)	15	[46]
$K_{AA,An}$ ($g.m^{-3}$)	14	[47]
$K_{NO2,H}$ ($g.m^{-3}$)	0.5	[47]
K_I ($g.m^{-3}$)	271	[44]
Y_H^{AA} ($g_X.g_{COD}^{-1}$)	0.67	[46]
Y_H ($g_X.g_{COD}^{-1}$)	0.6	[47]
Y_{AOB} ($g_X.g_{COD}^{-1}$)	0.15	[45]
η_{anox} (-)	0.8	[47]

2.5.4 MABR hydrodynamic model

In this study, the HRT of MABR is set to 12.5 h for all simulations. This is based on the findings of previous studies [48–50], which have indicated that Nitrogen treatment performances are strongly affected by HRT. On the one hand, HRT higher than 12 h may inhibit heterotrophic denitrification thus leading to nitrite and/or nitrate accumulation. On the other hand, HRT lower than 12 h and COD/N mass ratios higher than 4 may favor activity of heterotrophic rather than autotrophic bacteria, thus almost inhibiting nitrification [36,50]. Therefore, 12.5 h appears to be a suitable HRT value to obtain a well-developed autotrophic and heterotrophic biofilm. According to the inlet flow rate that is considered for the HPA stream (100 $m^3.h^{-1}$), a total

volume of 1,250 m^3 is required, thus leading to 4,310 MABR modules of volume equal to 0.29 m^3 and inlet flow equal to 0.023 $m^3.h^{-1}$ each.

The model of axial dispersion with slow exchange zones is used in this study to describe the internal hydrodynamics of each MABR module. Indeed, previous studies on MABR hydrodynamics have indicated that this model describes experimental retention time distribution data well [51]. The model consists in N series of cells each represented by two CSTR in parallel of volume V_1 and V_2 respectively, as shown in Fig. 3. V_1 represents the water volume of the slow exchange zone, whereas V_2 represents the water volume of the dynamic flow zone. For each series of cells, α represent the fraction of the inlet flow Q entering to the slow exchange zone of volume V_1. For the simulations, the MABR model is represented by an user module which uses the dynamic link library of the Fortran program.

Commenté [FJh2]: Si j'ai compris, il s'agit de la boudary layer et du bulk ?

Les réactions associées à chaque volume sont identiques ?

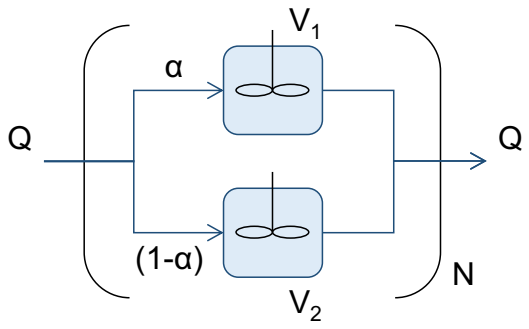

Fig. 3. Schematic view of the axial dispersion reactor with slow exchange zone model.

The number N of cells is calculated by Equations (18), where Pe represent the Peclet number of the dynamic flow zone [52]. Pe is determined by Equation (19), where ε represents the MABR void fraction (-), H is the height of the reactor (m), d_e is the effective reactor diameter (m), and Re_d the number of Reynolds associated to the dynamic flow zone [53,54]. The value of d_e is obtained by Equation (20), where d_R is the diameter of the reactor (m), d_f the outer diameter of the fibers (m), and n the number of fibers (-) [55]. The value of Re_d is calculated

by Equation (21), where u_d is the water velocity in the dynamic zone ($m.s^{-1}$), ν is the kinematic viscosity of water ($m^2.s^{-1}$), and d_e is the effective reactor diameter (m). The value of the void fraction ε of the MABR is set to 0.94 according to previous studies [56].

$$N = \frac{Pe}{2} + 1 \quad (18)$$

$$Pe = \frac{H}{\varepsilon \cdot d_e} \cdot \left(0.2 + 0.011 \cdot Re_d^{0.48}\right) \quad (19)$$

$$d_e = \frac{d_R^2 - n d_f^2}{d_R + d_f} \quad (20)$$

$$Re_d = \frac{u_d \cdot d_e}{\nu} \quad (21)$$

The fraction α of the inlet flow Q entering to the slow exchange zone of volume V_1 is determined by Equation (22) [29]. The ratio between the HRTs of V_1 and V_2 (τ_1/τ_2) is evaluated by Equation (23), where Fi represent the inlet mass flow per unit of surface of the reactor ($kg.m^{-2}.s^{-1}$). The ratio V_2/V_1 is evaluated by Equation (24), where q is the peripheral flow rate ($m^2.h^{-1}$) according to the hydraulic loading ($m.h^{-1}$) and the specific surface ($m^2.m^{-3}$) of the MABR. The Equations (23) and (24) are developed from experimental results published in the literature [52,56].

$$\alpha = \frac{1}{\frac{\tau_1}{\tau_2}\frac{V_2}{V_1} + 1} \quad (22)$$

$$\frac{\tau_1}{\tau_2} = -4.539 \cdot ln(Fi) + 15.902 \quad (23)$$

$$\frac{V_2}{V_1} = 12.33 \cdot q^{0.6054} \quad (24)$$

According to the geometric characteristics and inlet flow established for this simulation study, the calculated value of N, α, V_1, and V_2 are 4, 0.101, 0.056 m^3 and 0.017 m^3, respectively, thus for each MABR module.

2.6 Process schemes

Six different process schemes have been built and simulated: the conventional treatment scheme and five alternative treatment schemes.

Fig.4 summarizes the conventional HPA treatment scheme (HPA C) that consists of two successive precipitation steps to remove F, NH_4-N, and PO_4-P. As shown in Fig.4, F is precipitated as CaF_2 at pH 4, then NH_4-N and PO_4-P are removed by struvite precipitation at pH 8.8. For the first precipitation step, NaOH and $CaCl_2$ are used as OH^- and Ca^{2+} ions sources to regulate the pH at 4 and to precipitate CaF_2, respectively. For the second precipitation step, NaOH and $MgCl_2$ are used as OH^- and Mg^{2+} sources to increase pH at 8.8 and to precipitate struvite [9,57].

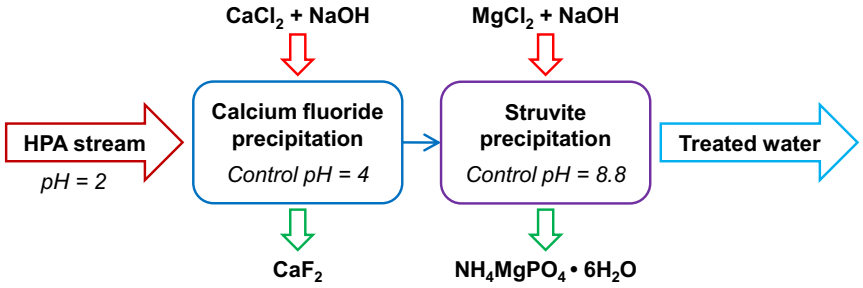

Fig. 4. Conventional treatment of HPA stream (HPA C).

Fig. 5 summarizes the three alternative HPA treatment schemes (HPA 1, HPA 2, and HPA 3) that are tested for effluent discharges to natural water. French national laws recommend effluent concentrations of COD, total N, and F lower than 125 g COD.m^{-3}, 30 g N.m^{-3}, and 15 g F.m^{-3}, respectively, for discharges to natural water (*Arrêté du 2 février 1998, article 32,* as modified by *Arrêté du 25 juin 2018*). Therefore, these effluent concentrations are used as target values for simulation of schemes HPA 1, HPA 2, and HPA 3. Each scheme consists of three consecutive treatment steps.

Fig.5a shows the first alternative process scheme (HPA 1). The Ca^{2+} and OH^- sources used in the conventional treatment scheme (HPA C) are replaced by hydrated lime ($Ca(OH)_2$). The advantage of $Ca(OH)_2$ compared to the conventional reagents is that its dissolution in water can simultaneously provide Ca^{2+} and OH^- ions to increase the pH at 4 and to enable CaF_2 precipitation in the first treatment step, thus reducing the total consumption of chemicals. Moreover, a further addition of $Ca(OH)_2$ and $MgCl_2$ provides the Mg^{2+} and OH^- ions to increase the pH at 8.8 and to enable struvite precipitation in the second treatment step. However, the ratio N/P of HPA stream is usually higher than the ratio N/P required for struvite precipitation, and the effluent from the struvite precipitation step still presents total N and COD concentrations higher than the limits established for discarding in natural waters. Therefore, an aerated activated sludge bioreactor (CSTR) is added as third treatment step to treat acetic acid and residual NH_4-N. The addition of acetic acid as external organic carbon is also considered to increase the COD/N ratio of the effluent, and hence to improve N uptake by upgrading biomass growth in the CSTR step.

Fig.5b shows the second alternative process scheme (HPA 2). The first and second treatment steps of HPA 2 (calcium fluoride and struvite precipitation, respectively) are identical to those of scheme HPA 1. Then, a MABR is added as third treatment step in scheme HPA 2 to further decrease total N and COD concentrations, and thus meet the standards for discarding in natural waters.

Fig.5c shows the third alternative process scheme (HPA 3). The first treatment step of scheme HPA 3 (calcium fluoride precipitation) is identical to those of schemes HPA 1 and HPA 2. Then, PO_4-P is removed by HAP precipitation at pH 8 by using $Ca(OH)_2$ as Ca^{2+} and OH^- ions source in the second treatment step. Finally, a MABR is added as third treatment step to further decrease total N and COD concentrations. However, the effluent from the hydroxyapatite precipitation step shows a lower ratio COD/N compared to the effluent of struvite precipitation,

as HAP precipitation does not involve NH_4-N removal. Therefore, the addition of acetic acid is considered in scheme HPA 3 to increase the ratio COD/N, and hence to improve denitrification performance.

As discussed in the results and discussion section, the simulations indicate that the treatment schemes HPA 1, HPA 2, and HPA 3 can meet the COD and total N standards for rejection to natural waters. However, total N concentrations of the effluents are still higher than the limit established for discharges to sensitive areas that are subject to eutrophication. Indeed, higher treatment standards for total N and total P (10 g $N.m^{-3}$ and 1 g $P.m^{-3}$, respectively) are required for discharges to sensitive areas. For these reasons, two additional alternative process schemes (HPA 4 and HPA 5) are proposed to improve N treatment (Fig. 6). As shown in Fig. 6a and b, the previous schemes HPA 2 and HPA 3 (Fig. 5b and c, respectively) are upgraded by the addition of an aerated CSTR as fourth treatment step to further decrease N concentrations by biological uptake (HPA 4 and HPA 5). The addition of acetic acid in the CSTR step is considered for both schemes to improve the ratio COD/N. Differently from scheme HPA 3, the addition of acetic acid in the MABR step is not considered for scheme HPA 5.

For all the struvite precipitation steps, the dose of $MgCl_2$ is based on the content of Ca^{2+} ions in the solutions, thus according to a molar ratio Ca/Mg of 0.053. This is done to limit HAP, FAP, and/or CaF_2 coprecipitation, and hence to improve the purity of the struvite crystals that are recovered [58]. For all the bioconversion steps requiring the addition of external organic carbon (CSTR and MABR steps), the optimum dose of acetic acid is determined by iterative simulations. All simulations are performed according to standard temperature and pressure conditions (25 °C and 0.1 MPa).

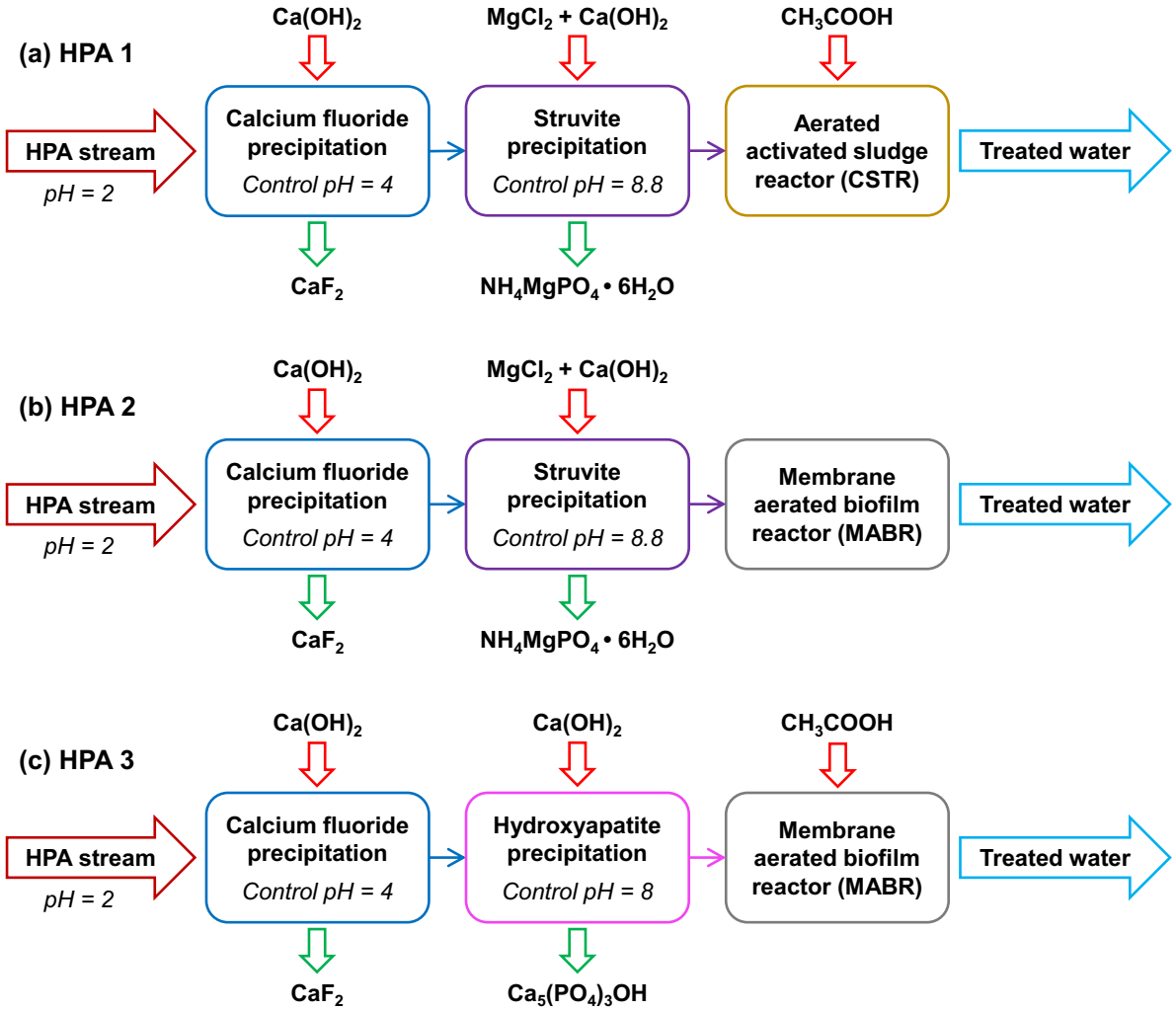

Fig. 5. Alternative HPA treatment schemes for discharges to natural water: (a) HPA 1; (b) HPA 2; (c) HPA 3.

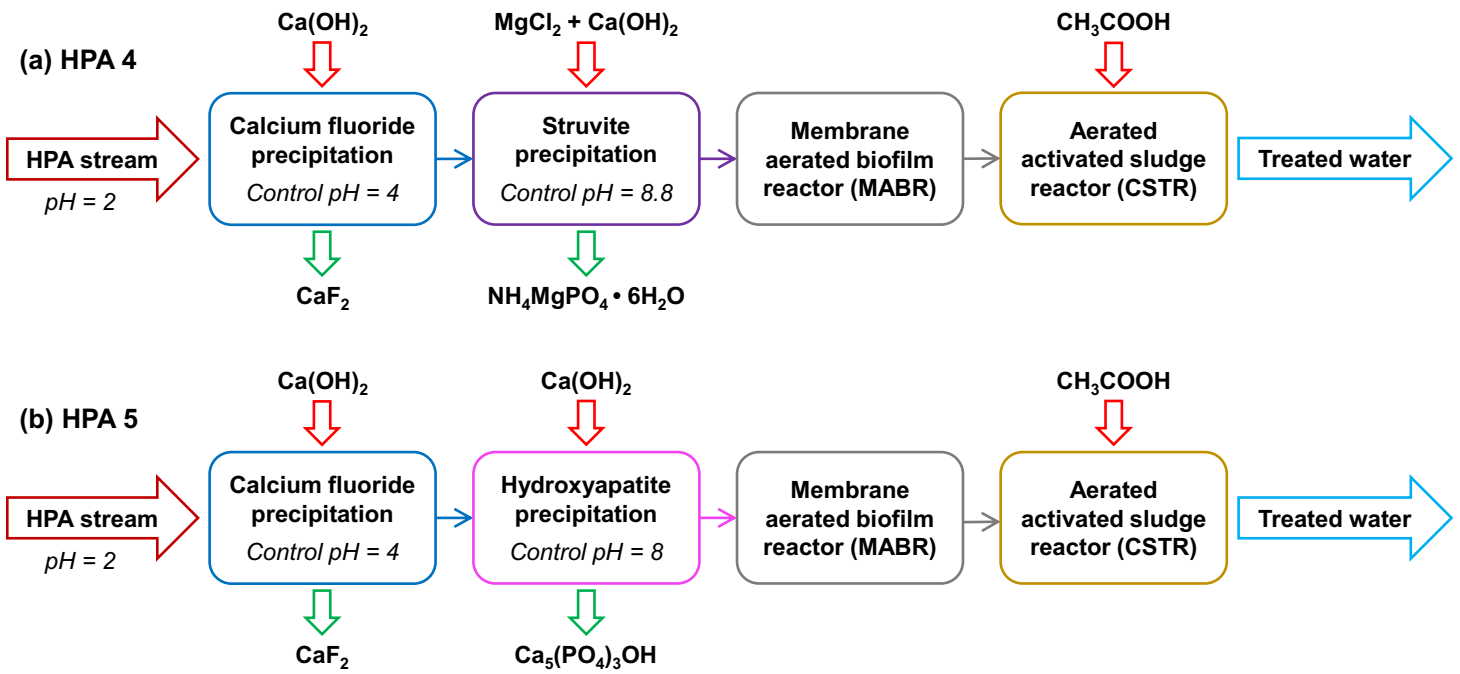

Fig. 6. Alternative HPA treatment schemes for discharges to sensitive areas: (a) HPA 4; (b) HPA 5.

3. Results and discussion

3.1 Effluent quality

The simulated COD, N, F, and P effluent concentrations for the different HPA treatment schemes are summarized in Table 5. The concentrations of F and P of the effluents meet the limits for discharge to natural water for all the HPA treatment schemes. For the conventional HPA treatment scheme (HPA C), the outlet F concentration is directly controlled by the addition of $CaCl_2$ as the only source of Ca^{2+} ions to enable CaF_2 precipitation. On the contrary, for all other schemes, the use of $Ca(OH)_2$ as source of OH^- ions to control the pH provides a higher amount of Ca^{2+} ions that are available for CaF_2 precipitation, thus giving lower F concentrations. The results also indicate that outlet F concentration depends on the treatment scheme. For all schemes, most of F is removed during the first precipitation step. In schemes HPA 1, 2, and 4, a further amount of F is removed by CaF_2 precipitation in the struvite precipitation step, thus giving an outlet F concentration of 8.3 g $F.m^{-3}$. For schemes HPA 3 and 5, FAP precipitation in the hydroxyapatite precipitation step further reduces outlet F concentration to 0 g $F.m^{-3}$. Indeed, the solubility of FAP at pH 8 is one order of magnitude lower than that of HAP [59], and high purity HAP precipitation occurs only when the concentration of F^- ions are limiting FAP precipitation.

The results of simulations indicate that COD and total N concentrations of the effluent from scheme HPA C (321 g $COD.m^{-3}$ and 83 g $N.m^{-3}$) do not meet the standards for discharge to natural water (125 g $COD.m^{-3}$ and 30 g $N.m^{-3}$). Instead, outlet COD and total N concentrations for schemes HPA 1 (44.6 g $COD.m^{-3}$ and 29.9 g $N.m^{-3}$) and HPA 2 (57.5 g $COD.m^{-3}$ and 21 g $N.m^{-3}$) meet the standards. Differently from the previous schemes, the effluent from scheme HPA 3 meets the standard for total N but not for COD, as its outlet COD concentration (182 g $COD.m^{-3}$) is still higher than the limit value for discharge to natural water. This suggests that MABR is more suitable after the struvite rather than after the hydroxyapatite precipitation step, most probably because the consumption of N for struvite precipitation leads to effluents with

Commenté [FJh3]: J'ai toujours la mm question, est ce que si on augmenatit V on améliorearit ou pas ?

lower NH_4-N concentrations and a more suitable COD/N ratio for partial nitrification followed by heterotrophic denitrification. Increasing HRT of MABR beyond 12.5 h could be a solution to complete conversion reactions and hence to increase total N and COD removal performances of scheme HPA 3. However, this would lead to an increase of the total volume needed for the MABR above 1,250 m^{-3} by the addition of additional MABR modules. Moreover, in the practice the increase in HRT beyond 12.5 h may favor the growth of autotrophic rather than heterotrophic bacteria, thus finally decreasing the COD treatment performance [36].

Commenté [FJh4]: Plus haut tu as écrit :

HRT higher than 12 h may inhibit heterotrophic denitrification thus leading to nitrite and/or nitrate accumulation.

Est ec que ca n'est pas contardictoire ?

As shown in Table 5, the addition of an aerated CSTR as final treatment step in schemes HPA 4 and HPA 5 can further reduce COD and total N concentrations of the effluents to 3-6.2 g COD.m^{-3} and 9.4 g N.m^{-3}, respectively, thus allowing effluent discharge to sensitive areas that are subject to eutrophication.

Table 5. Simulated effluent quality for the different HPA treatment schemes.

Parameter	**Treatment scheme**					
	HPA C	**HPA 1**	**HPA 2**	**HPA 3**	**HPA 4**	**HPA 5**
COD (g.m^{-3})	321	44.6	57.5	182	3	6.2
Total N (g.m^{-3})	83	29.9	21	29.6	9.4	9.4
Total P (g.m^{-3})	1.66	0	0	0	0	0
Total F (g.m^{-3})	13.7	8.3	8.3	0	8.3	0

3.2 Consumption of chemical reagents

The consumption of chemical reagents is one the factors to be considered for a further economic evaluation. The simulated consumptions of chemical reagents for the different HPA schemes are summarized in Table 6. The results indicate that the conventional treatment HPA C requires

the highest chemical consumption. As shown in Table 6, HPA C requires 3,600 $g.m^{-3}$ of $CaCl_2$ for the calcium fluoride precipitation step, 14,000 $g.m^{-3}$ of $MgCl_2$ for the struvite precipitation step, and 3,150 $g.m^{-3}$ of NaOH (2600 $g.m^{-3}$ of NaOH for the calcium fluoride precipitation step, and 550 $g.m^{-3}$ of NaOH for the struvite precipitation step).

As shown in Table 6, the total chemical consumption is significantly reduced by the replacement of $CaCl_2$ and NaOH with $Ca(OH)_2$ in all the alternative schemes (Fig. 5 and 6). Among the different treatment steps, struvite precipitation shows the highest consumption of chemicals. Indeed, in the presence of Ca^{2+} ions, struvite precipitation is in competition with Ca-phosphate precipitation, and its precipitation efficiency depends on the ratio between Ca and Mg ions that are available in the solution (Ca/Mg ratio): the higher the Ca/Mg ratio, the lower struvite precipitation efficiency. Therefore, a dose of $MgCl_2$ higher than the stoichiometric dose is usually required for an efficient struvite precipitation [58]. The results of Liu and Wang [58] indicate that molar ratios Ca/Mg higher than 0.5 are inappropriate to obtain struvite crystals with high purity. According to the data of Hanhoun [60] the Ca/Mg ratio is fixed at 0.053 mol Ca/mol Mg for the simulations of struvite precipitation steps, thus giving a simulated consumption of 14,000 g $MgCl_2.m^{-3}$. In addition to $MgCl_2$, struvite precipitation step requires 520 $g.m^{-3}$ of $Ca(OH)_2$ as OH^- source to regulate the pH at 8.8.

The schemes HPA 3 and HPA 5, where the struvite precipitation step is replaced by the hydroxyapatite precipitation step, give the lowest total consumption of chemical reagents (3,368 and 3,190 $g.m^{-3}$, respectively). Indeed, hydroxyapatite precipitation step requires only the addition of 510 $g.m^{-3}$ of $Ca(OH)_2$ as Ca^{2+} and OH^- ions source to regulate the pH at 8 and to enable HAP precipitation. Among the different alternative schemes, HPA 2 is the only one that does not require the addition of external organic carbon (acetic acid) to achieve an outlet total N concentration below 30 mg $N.m^{-3}$. For the schemes HPA 1, HPA 3, HPA 4, and HPA 5, several tests were performed to determine the optimum dose of acetic acid required to

upgrade N removal in the bioconversion processes (CSTR and/or MABR steps). The results indicate that scheme HPA 1 requires the highest dose of acetic acid (800 $g.m^{-3}$) whereas scheme HPA 4 requires the lowest dose of acetic acid (200 $g.m^{-3}$).

Table 6. Simulated consumption of chemical reagents for the different HPA treatment schemes.

Chemical reagents	**Treatment scheme**					
	HPA C	**HPA 1**	**HPA 2**	**HPA 3**	**HPA 4**	**HPA 5**
$CaCl_2$ ($g.m^{-3}$)	3,600	-	-	-	-	-
NaOH ($g.m^{-3}$)	3,150	-	-	-	-	-
$MgCl_2$ ($g.m^{-3}$)	14,000	14,000	14,000	-	14,000	-
$Ca(OH)_2$ ($g.m^{-3}$)	-	2,930	2,930	2,920	2,930	2,920
CH_3COOH ($g.m^{-3}$)	-	800	-	448	200	270
TOTAL ($g.m^{-3}$)	20,750	17,730	16,930	3,368	17,130	3,190

3.3 Recovery of chemical by-products

Table 7 summarizes the simulated amounts of by-products and the chemical compositions of the precipitates that are recovered from the steps of calcium fluoride, struvite, and hydroxyapatite precipitation. The results indicate that 1,921 $g.m^{-3}$ of CaF_2 with a theoretical purity of 100% can be recovered from the first step of calcium fluoride precipitation for all the treatment schemes. The recovery of high grade CaF_2 (purity > 97%) is very interesting, as it represent a high value by product that can be reused in several industrial applications, including the production of hydrofluoric acid, the manufacture of glasses, and the iron and steel industry [12].

Table 7. Simulated recovery of chemical by-products for the different HPA treatment schemes: HAP = hydroxyapatite; FAP = fluorapatite.

Precipitation step	Chemical by-products	Treatment scheme					
		HPA C	HPA 1	HPA 2	HPA 3	HPA 4	HPA 5
Calcium fluoride precipitation	CaF_2 ($g.m^{-3}$)	1,921	1,921	1,921	1,921	1,921	1,921
Struvite precipitation	CaF_2 ($g.m^{-3}$)	--	11	11	--	11	--
	Struvite ($g.m^{-3}$)	992	992	992	--	992	--
	FAP ($g.m^{-3}$)	5.83	4.75	4.75	--	4.75	--
Hydroxyapatite precipitation	FAP ($g.m^{-3}$)	--	--	--	375	--	375
	HAP ($g.m^{-3}$)	--	--	--	304	--	304

Moreover, 992 $g.m^{-3}$ of struvite and 375 $g.m^{-3}$ of HAP can be recovered from the struvite and hydroxyapatite precipitation steps, respectively. However, residual F from the calcium fluoride precipitation step can react with Ca^{2+} ions to form CaF_2 and/or FAP, thus decreasing the purity of the precipitates that are recovered from the struvite and hydroxyapatite precipitation steps. According to the data in Table 7, the highest purity of precipitates recovered from the struvite precipitation step is observed for the conventional scheme HPA C (struvite purity 99.4%), whereas the alternative schemes HPA 1, HPA 2, and HPA 4 give a slight lower value of struvite purity (98.4%). This because the higher concentrations of Ca^{2+} ions due to the addition of $Ca(OH)_2$ favors coprecipitation of CaF_2 and FAP in the struvite precipitation step, thus decreasing the purity of the precipitates. The purity of HAP in the precipitates recovered from the hydroxyapatite precipitation steps in schemes HPA 3 and HPA 5 is equal to 44.8%.

Struvite and HAP represent high value by-products that can be reused in agriculture as an effective source of N and/or P for plant growth, or in the industry as a secondary raw material for the production of fertilizers [61]. The results in Table 7 indicate that the precipitates from struvite and hydroxyapatite precipitation steps may contain other minerals (CaF_2 and FAP), and they present a F content ranging from 0.22 g $F.kg^{-1}$ for scheme HPA C to 20.8 mg $F.kg^{-1}$ for scheme HPA 3 and HPA 5. Nowadays, European legislation governing P recovery and recycling as fertilizer does not set a limit value for F content for application on agricultural lands [62]. Therefore, the results of simulations suggest that the precipitates recovered from the struvite and hydroxyapatite precipitation steps can be directly reuse as fertilizers in the fields.

However, it should be mentioned that the quality grade and hence the resale price of the precipitates strongly depend on their purity [62]. In schemes HPA 3 and HPA 5, the division of the second step into separate steps to precipitate first FAP, and then HAP, can give precipitates with a high purity degree that could be valorized in advanced technical applications (*e.g.* manufacture of dental prostheses).

In schemes HPA 1, HPA 2, and HPA 4, the addition of $CaCl_2$ in the calcium fluoride precipitation step can further remove F by a supplementary CaF_2 precipitation, thus limiting the precipitation of CaF_2 and FAP in the struvite precipitation step. Indeed, $CaCl_2$ dissolution provides supplementary Ca^{2+} ions that are available for further CaF_2 without modifying the pH of the solution.

A sensitivity analysis of the precipitation modules of schemes HPA 1, HPA 2, and HPA 4 was performed to evaluate the effect of different doses of $CaCl_2$ (added in the first precipitation step) on the purity and on the amount of CaF_2 and struvite recovered from the first and from the second precipitation steps, respectively. Four different $CaCl_2$ doses were tested, 0, 6, 8, and 15 kg $CaCl_2.m^{-3}$. Fig. 7a indicates that the increase of $CaCl_2$ dose from 0 to 6 kg $CaCl_2.m^{-3}$ leads to an increase in struvite purity from 98.3 to 99.4%, while CaF_2 purity decreases from 100

to 99.9%. This because the higher Ca^{2+} ion concentration in the first precipitation leads to coprecipitation of FAP with CaF_2, thus decreasing the purity of the precipitates. Moreover, a further increase in $CaCl_2$ dose to 8 kg $CaCl_2.m^{-3}$ results in a further decrease of CaF_2 purity to 87.2% while the struvite purity decreases to 99%. Also, the results in Fig. 7b indicate that the increase in $CaCl_2$ dose over 6 kg $CaCl_2.m^{-3}$ leads to a decrease in the amount of struvite that is recovered from the second precipitation step. Indeed, the increase in $CaCl_2$ dose results in a higher amount of FAP that is precipitated in the first precipitation step, thus decreasing the amount of P that is available for struvite precipitation in the second precipitation step. Overall, the results seem to indicate that 6 kg $CaCl_2.m^{-3}$ is the optimum dose to improve struvite purity while limiting the decrease in CaF_2 purity of the precipitates that are recovered from the second and from the first precipitation step, respectively.

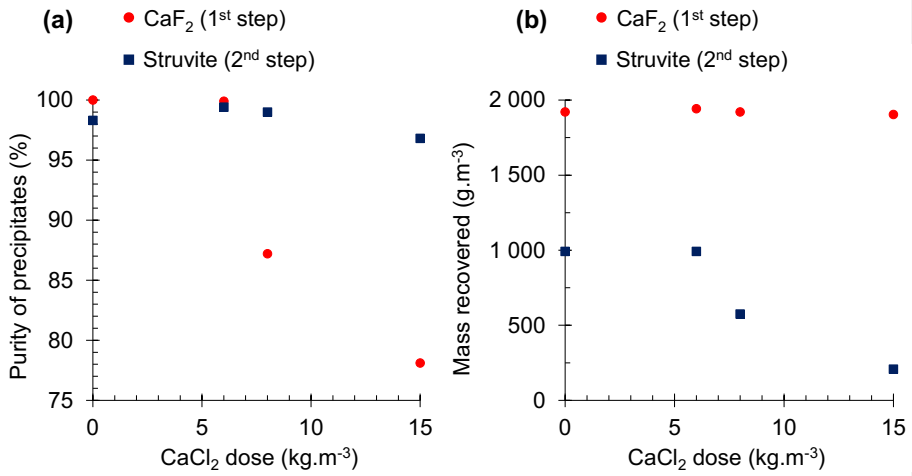

Fig. 7. Effect of different doses of $CaCl_2$ on the purity (a) and on the amount (b) of precipitates recovered from the 1st and from the 2nd precipitation steps (schemes HPA 1, HPA 2, and HPA 4).

4. Conclusions

Five alternative treatment schemes, based on the integration of innovative chemical precipitation and biological treatment processes, are simulated to evaluate their treatment performance of HPA stream from microelectronic industry.

The results indicate that the replacement of $CaCl_2$ and NaOH with $Ca(OH_2)$ as the only source of Ca^{2+} and OH^- ions for the precipitation steps is a promising way to reduce the total consumption of chemical reagents. Moreover, the use of a MABR after the precipitation steps appears to be a suitable technical solution to further decrease the COD and total N concentrations of the effluents. The results from comparative simulations suggest that scheme HPA 2 (calcium chloride precipitation, followed by struvite precipitation, followed by a MABR) is the most suitable treatment scheme for discharges to natural waters, and it allows reducing the total consumption of chemical reagents while recovering high purity (> 98%) CaF_2 and struvite. The addition of a supplementary aerobic CSTR may further reduce outlet COD and total N concentrations, thus allowing effluent discharge to sensitive areas that are subject to eutrophication. This study also contributes to the development of chemical precipitation and biological treatment modules that can be further applied for simulation studies on different types of wastewaters (*e.g.* agricultural and domestic wastewater, effluents from food, painting, textile, pharmaceutical industries). Overall, the results of this study give useful information for the development of innovative treatment processes, and they provide crucial data for the selection of the most promising alternative schemes. However, further experimental studies at the pilot scale are required to evaluate the treatment performances under real operative conditions before to apply the selected process schemes at the full operative scale.

Nomenclature

$\mathbf{A_F}$ Total biofilm surface area, (m^2)

$\mathbf{C_{in}^S}$ Substrate concentration in the influent, ($g.m^{-3}$)

C_B^S Substrate concentration in bulk liquid, ($g.m^{-3}$)

C_F^S Substrate concentration at the biofilm/boundary layer interface, ($g.m^{-3}$)

Cp^S Solid specific heat capacity, ($J.mol^{-1}.K^{-1}$)

d_e Effective diameter, (m)

d_f Fiber diameter, (m)

d_R Reactor diameter, (m)

D_L^S Substrate diffusion coefficient in water, ($m^2.s^{-1}$)

D_F^S Substrate diffusion coefficient in biofilm, ($m^2.s^{-1}$)

Fi Inlet mass flow per unit of surface, ($kg.m^{-2}.s^{-1}$)

Hf Fiber length, (m)

j_F^S Substrate flux, ($g.m^{-2}.s^{-1}$)

Ks Solubility constant ($mol.L^{-1}$)

$K_{NH4,AOB}$ Ammonium affinity constant, ($g.m^{-3}$)

K_I Ammonium inhibition constant, ($g.m^{-3}$)

$K_{AA,A}$ Acetic acid aerobic affinity constant, ($g.m^{-3}$)

$K_{NO2,H}$ Nitrite affinity constant, ($g.m^{-3}$)

$K_{AA,An}$ Acetic acid anaerobic affinity constant, ($g.m^{-3}$)

k_S Substrate mass transfer coefficient, ($m.s^{-1}$)

k_{NH4} Ammonium mass transfer coefficient, ($m.s^{-1}$)

L_F Biofilm thickness, (m)

L_L Boundary layer thickness, (m)

n Fiber number, (-)

Pe Péclet number, (-)

q Peripheral flow rate, ($m^2.h^{-1}$)

r_S Substrate consumption rate, ($g.m^{-3}.s^{-1}$)

Re	Reynolds number, (-)
R_N	Assimilation yield, ($g_{N\text{-}NH4}.g_{COD}^{-1}$)
u_d	Water velocity in the dynamic flow zone, ($m.s^{-1}$)
V	Reactor volume, (m^3)
V_1	Slow exchange zone volume, (m^3)
V_2	Dynamic flow zone volume, (m^3)
X_{AOB}	AOB biofilm density, ($g.m^{-3}$)
X_H	Heterotrophic biofilm density, ($g.m^{-3}$)
X	Biofilm density, ($g.m^{-3}$)
Y_{AOB}	Autotrophic (AOB) biomass yield, ($g_X.g_{COD}^{-1}$)
Y	Heterotrophic biomass yield, ($g_X.g_{COD}^{-1}$)
Y_H	Heterotrophic denitrifying yield, ($g_X.g_{COD}^{-1}$)
z	Distance from packing, (m)
α	Fraction of the inlet flow entering to the slow exchange zone, (-)
ε	Void fraction of the MABR, (-)
η^H_{anox}	Anoxic reduction factor for denitrifying biomass, (-)
μ_{max}	Specific growth rate, (h^{-1})
μ_{max}^{AOB}	Specific growth rate of AOB, (d^{-1})
$\mu_{max,}^{AA}$	Specific growth rate of heterotrophic biomass with acetic acid, (d^{-1})
μ_{maxH}	Specific growth rate of denitrifying biomass, (d^{-1})
ν	Kinematic viscosity of water, ($m^2.s^{-1}$)
τ_1	Hydraulic retention time associated to the slow exchange zone, (h)
τ_2	Hydraulic retention time associated to the dynamic flow zone, (h)

Acknowledgment

The authors thank the French Ministry of Research for the PhD grant support.

References

[1] A. Villard, A. Lelah, D. Brissaud, Drawing a chip environmental profile: environmental indicators for the semiconductor industry, Journal of Cleaner Production. 86 (2015) 98–109. https://doi.org/10.1016/j.jclepro.2014.08.061.

[2] I. Baudry, A. Lelah, D. Brissaud, Data Collection of Chemicals Used in Microelectronic Manufacturing Processes for Environmental Studies, in: D.A. Dornfeld, B.S. Linke (Eds.), Leveraging Technology for a Sustainable World, Springer, Berlin, Heidelberg, 2012: pp. 521–526. https://doi.org/10.1007/978-3-642-29069-5_88.

[3] C.-J.M. Chin, P.-W. Chen, L.-J. Wang, Removal of nanoparticles from CMP wastewater by magnetic seeding aggregation, Chemosphere. 63 (2006) 1809–1813. https://doi.org/10.1016/j.chemosphere.2005.09.035.

[4] H. Huang, J. Liu, P. Zhang, D. Zhang, F. Gao, Investigation on the simultaneous removal of fluoride, ammonia nitrogen and phosphate from semiconductor wastewater using chemical precipitation, Chemical Engineering Journal. 307 (2017) 696–706. https://doi.org/10.1016/j.cej.2016.08.134.

[5] H.-D. Ryu, D. Kim, S.-I. Lee, Application of struvite precipitation in treating ammonium nitrogen from semiconductor wastewater, Journal of Hazardous Materials. 156 (2008) 163–169. https://doi.org/10.1016/j.jhazmat.2007.12.010.

[6] J.-Y. Kim, C.-H. Shin, H. Choi, W. Bae, Recovery of phosphoric acid from mixed waste acids of semiconductor industry by diffusion dialysis and vacuum distillation, Separation and Purification Technology. 90 (2012) 64–68. https://doi.org/10.1016/j.seppur.2012.02.013.

[7] N. Martin, V. Ya, N. Leewiboonsilp, K.-H. Choo, P. (Lek) Noophan, C.-W. Li, Electrochemical crystallization for phosphate recovery from an electronic industry wastewater effluent using sacrificial iron anodes, Journal of Cleaner Production. 276 (2020) 124234. https://doi.org/10.1016/j.jclepro.2020.124234.

[8] K. Ohanessian, M. Monnot, P. Moulin, J.-H. Ferrasse, C. Barca, A. Soric, O. Boutin, Dead-end and crossflow ultrafiltration process modelling: Application on chemical mechanical polishing wastewaters, Chemical Engineering Research and Design. 158 (2020) 164–176. https://doi.org/10.1016/j.cherd.2020.04.007.

[9] Y.-J. Shih, R.R.M. Abarca, M.D.G. de Luna, Y.-H. Huang, M.-C. Lu, Recovery of phosphorus from synthetic wastewaters by struvite crystallization in a fluidized-bed reactor: Effects of pH, phosphate concentration and coexisting ions, Chemosphere. 173 (2017) 466–473. https://doi.org/10.1016/j.chemosphere.2017.01.088.

[10] D.K. James, A.J. Gerbino, Using Process Simulation to Predict Wastewater Treatment Outcomes, Semiconductor Pure Water and Chemicals Conference, Pp. 206-237, Mar. 2000, Santa. Clara, CA. (2000) 30.

[11] Warmadewanthi, J.C. Liu, Recovery of phosphate and ammonium as struvite from semiconductor wastewater, Separation and Purification Technology. 64 (2009) 368–373. https://doi.org/10.1016/j.seppur.2008.10.040.

[12] R. Aldaco, A. Garea, A. Irabien, Calcium fluoride recovery from fluoride wastewater in a fluidized bed reactor, Water Research. 41 (2007) 810–818. https://doi.org/10.1016/j.watres.2006.11.040.

[13] G. Jia, H. Zhang, J. Krampe, T. Muster, B. Gao, N. Zhu, B. Jin, Applying a chemical equilibrium model for optimizing struvite precipitation for ammonium recovery from anaerobic digester effluent, Journal of Cleaner Production. 147 (2017) 297–305. https://doi.org/10.1016/j.jclepro.2017.01.116.

[14] T. Pavón-Silva, V. Pacheco-Salazar, J.C. Sánchez-Meza, G. Roa-Morales, A. Colín-Cruz, Physicochemical and biological combined treatment applied to a food industry wastewater for reuse, Journal of Environmental Science and Health, Part A. 44 (2009) 108–115. https://doi.org/10.1080/10934520802515467.

[15] M. Riera-Torres, C. Gutiérrez-Bouzán, Optimisation of the electrochemical and UV combined treatment to remove colour and organic halogenated compounds of textile effluents, Separation and Purification Technology. 98 (2012) 375–382. https://doi.org/10.1016/j.seppur.2012.08.005.
[16] P.A. Soloman, C. Ahmed Basha, M. Velan, N. Balasubramanian, P. Marimuthu, Augmentation of biodegradability of pulp and paper industry wastewater by electrochemical pre-treatment and optimization by RSM, Separation and Purification Technology. 69 (2009) 109–117. https://doi.org/10.1016/j.seppur.2009.07.002.
[17] J. Vidal, C. Huiliñir, R. Salazar, Removal of organic matter contained in slaughterhouse wastewater using a combination of anaerobic digestion and solar photoelectro-Fenton processes, Electrochimica Acta. 210 (2016) 163–170. https://doi.org/10.1016/j.electacta.2016.05.064.
[18] M.D.G. de Luna, Warmadewanthi, J.C. Liu, Combined treatment of polishing wastewater and fluoride-containing wastewater from a semiconductor manufacturer, Colloids and Surfaces A: Physicochemical and Engineering Aspects. 347 (2009) 64–68. https://doi.org/10.1016/j.colsurfa.2008.12.006.
[19] C.Y. Eng, D. Yan, N. Withanage, Q. Liang, Y. Zhou, Wastewater treatment and recycle from a semiconductor industry: A demo-plant study, Water Practice and Technology. 14 (2019) 371–379. https://doi.org/10.2166/wpt.2019.020.
[20] E.L. Shock, H.C. Helgeson, D.A. Sverjensky, Calculation of the thermodynamic and transport properties of aqueous species at high pressures and temperatures: Standard partial molal properties of inorganic neutral species, Geochimica et Cosmochimica Acta. 53 (1989) 2157–2183. https://doi.org/10.1016/0016-7037(89)90341-4.
[21] A. La Iglesia, Estimating the thermodynamic properties of phosphate minerals at high and low temperature from the sum of constituent units, Estudios Geológicos. (2009) 109–119. https://doi.org/10.3989/egeol.39849.060.
[22] A.V. Chichagov, D.A. Varlamov, R.A. Dilanyan, T.N. Dokina, N.A. Drozhzhina, O.L. Samokhvalova, T.V. Ushakovskaya, MINCRYST: A crystallographic database for minerals, local and network (WWW) versions, Crystallogr. Rep. 46 (2001) 876–879. https://doi.org/10.1134/1.1405882.
[23] J.E. Hurst, B.K. Harrison, Estimation of liquid and solid heat capacities using a modified Kopp's rule, Chemical Engineering Communications. 112 (1991) 21–30. https://doi.org/10.1080/00986449208935989.
[24] R.A. Robie, B.S. Hemingway, G. Survey (U.S.), Thermodynamic Properties of Minerals and Related Substances at 298.15 K and 1 Bar (105 Pascals) Pressure and at Higher Temperatures, U.S. Government Printing Office, 1995.
[25] E.L. Shock, H.C. Helgeson, Calculation of the thermodynamic and transport properties of aqueous species at high pressures and temperatures: Correlation algorithms for ionic species and equation of state predictions to 5 kb and 1000°C, Geochimica et Cosmochimica Acta. 52 (1988) 2009–2036. https://doi.org/10.1016/0016-7037(88)90181-0.
[26] M.I.H. Bhuiyan, D.S. Mavinic, R.D. Beckie, A Solubility and Thermodynamic Study of Struvite, Environmental Technology. 28 (2007) 1015–1026. https://doi.org/10.1080/09593332808618857.
[27] H. McDowell, T.M. Gregory, W.E. Brown, Solubility of Ca5(PO4)3OH in the system Ca(OH)2-H3PO4-H2O at 5, 15, 20 and 37 °C, JOURNAL OF RESEARCH of the National Bureau of Standards- A. Physics and Chemistry. 81A (1977) 273–281.
[28] M. Spérandio, M. Heran, S. Gillot, Modélisation dynamique des procédés biologiques de traitement des eaux., Techniques de l'Ingénieur. (2007) 1–18.
[29] M. Minière, A. Soric, O. Boutin, Experimental coupling and modelling of wet air oxidation and packed-bed biofilm reactor as an enhanced phenol removal technology, Environmental Science and Pollution Research. 24 (2017) 7693–7704.

[30] B. Guieysse, Z.N. Norvill, Sequential chemical–biological processes for the treatment of industrial wastewaters: Review of recent progresses and critical assessment, Journal of Hazardous Materials. 267 (2014) 142–152. https://doi.org/10.1016/j.jhazmat.2013.12.016.
[31] S. Matsumoto, A. Terada, S. Tsuneda, Modeling of membrane-aerated biofilm: Effects of C/N ratio, biofilm thickness and surface loading of oxygen on feasibility of simultaneous nitrification and denitrification, Biochemical Engineering Journal. 37 (2007) 98–107. https://doi.org/10.1016/j.bej.2007.03.013.
[32] K. Hibiya, A. Terada, S. Tsuneda, A. Hirata, Simultaneous nitrification and denitrification by controlling vertical and horizontal microenvironment in a membrane-aerated biofilm reactor, Journal of Biotechnology. 100 (2003) 23–32. https://doi.org/10.1016/S0168-1656(02)00227-4.
[33] M. González-Brambila, O. Monroy, F. López-Isunza, Experimental and theoretical study of membrane-aerated biofilm reactor behavior under different modes of oxygen supply for the treatment of synthetic wastewater, Chemical Engineering Science. 61 (2006) 5268–5281. https://doi.org/10.1016/j.ces.2006.03.049.
[34] A. Terada, K. Hibiya, J. Nagai, S. Tsuneda, A. Hirata, Nitrogen removal characteristics and biofilm analysis of a membrane-aerated biofilm reactor applicable to high-strength nitrogenous wastewater treatment, Journal of Bioscience and Bioengineering. 95 (2003) 170–178. https://doi.org/10.1016/S1389-1723(03)80124-X.
[35] M. Chaali, M. Naghdi, S.K. Brar, A. Avalos-Ramirez, A review on the advances in nitrifying biofilm reactors and their removal rates in wastewater treatment: A review on the advances of nitrifying biofilm reactors and their removal rates in wastewater treatment, J. Chem. Technol. Biotechnol. 93 (2018) 3113–3124. https://doi.org/10.1002/jctb.5692.
[36] M. Li, C. Du, J. Liu, X. Quan, M. Lan, B. Li, Mathematical modeling on the nitrogen removal inside the membrane-aerated biofilm dominated by ammonia-oxidizing archaea (AOA): Effects of temperature, aeration pressure and COD/N ratio, Chemical Engineering Journal. 338 (2018) 680–687. https://doi.org/10.1016/j.cej.2018.01.040.
[37] N. Bernet, P. Dangcong, J.-P. Delgenès, R. Moletta, Nitrification at Low Oxygen Concentration in Biofilm Reactor, Journal of Environmental Engineering. 127 (2001) 266–271. https://doi.org/10.1061/(ASCE)0733-9372(2001)127:3(266).
[38] R. Blackburne, Z. Yuan, J. Keller, Partial nitrification to nitrite using low dissolved oxygen concentration as the main selection factor, Biodegradation. 19 (2008) 303–312. https://doi.org/10.1007/s10532-007-9136-4.
[39] W. Jianlong, Y. Ning, Partial nitrification under limited dissolved oxygen conditions, Process Biochemistry. 39 (2004) 1223–1229. https://doi.org/10.1016/S0032-9592(03)00249-8.
[40] L.-S. Fan, R. Leyva-Ramos, K.D. Wisecarver, B.J. Zehner, Diffusion of phenol through a biofilm grown on activated carbon particles in a draft-tube three-phase fluidized-bed bioreactor, Biotechnology and Bioengineering. 35 (1990) 279–286. https://doi.org/10.1002/bit.260350309.
[41] K. Hibiya, J. Nagai, S. Tsuneda, A. Hirata, Simple prediction of oxygen penetration depth in biofilms for wastewater treatment, Biochemical Engineering Journal. 19 (2004) 61–68. https://doi.org/10.1016/j.bej.2003.10.003.
[42] O. Wanner, H.J. Ebert, E. Morgenroth, D. Noguera, C. Picioreanu, B.E. Rittmann, M.C.M. Van Loosdrecht, Mathematical modeling of biofilms, IWA Pub., 2006. https://agris.fao.org/agris-search/search.do?recordID=US201300120281 (accessed May 9, 2021).
[43] J. Dosta, A. Galí, T. Benabdallah El-Hadj, S. Macé, J. Mata-Álvarez, Operation and model description of a sequencing batch reactor treating reject water for biological nitrogen removal via nitrite, Bioresource Technology. 98 (2007) 2065–2075. https://doi.org/10.1016/j.biortech.2006.04.033.
[44] J. Pérez, E. Costa, J.-U. Kreft, Conditions for partial nitrification in biofilm reactors and a kinetic explanation, Biotechnol. Bioeng. 103 (2009) 282–295. https://doi.org/10.1002/bit.22249.
[45] M. Zeng, A. Soric, N. Roche, Modeling partial nitrification and denitrification in a hybrid biofilm reactor: calibration by retention time distribution and respirometric tests, Environ Sci Pollut Res. 22 (2015) 12849–12860. https://doi.org/10.1007/s11356-014-3667-0.

[46] M. Minière, Etude du couplage d'un procédé d'oxydation en voie humide et d'un bioprocédé à biofilm aérobie en lit fixe pour le traitement de composés organiques réfractaires aux traitements conventionnels, PhD Thesis, Aix-Marseille University, France, 2016. https://www.theses.fr/2016AIXM4375 (accessed October 31, 2021).
[47] G. Sin, D. Kaelin, M.J. Kampschreur, I. Takács, B. Wett, K.V. Gernaey, L. Rieger, H. Siegrist, M.C.M. van Loosdrecht, Modelling nitrite in wastewater treatment systems: a discussion of different modelling concepts, Water Science and Technology. 58 (2008) 1155–1171. https://doi.org/10.2166/wst.2008.485.
[48] N. Landes, A. Rahman, A. Morse, W.A. Jackson, Performance of a lab-scale membrane aerated biofilm reactor treating nitrogen dominant space-based wastewater through simultaneous nitrification-denitrification, Journal of Environmental Chemical Engineering. 9 (2021) 104644. https://doi.org/10.1016/j.jece.2020.104644.
[49] S. Mehrabi, D. Houweling, M. Dagnew, Establishing mainstream nitrite shunt process in membrane aerated biofilm reactors: Impact of organic carbon and biofilm scouring intensity, Journal of Water Process Engineering. 37 (2020) 101460. https://doi.org/10.1016/j.jwpe.2020.101460.
[50] N.H.S.M. Premarathna, C. Visvanathan, Enhancement of organic matter and total nitrogen removal in a membrane aerated biofilm reactor using PVA-Gel bio-carriers, Bioresource Technology Reports. 8 (2019) 100325. https://doi.org/10.1016/j.biteb.2019.100325.
[51] R. Plascencia-Jatomea, F.J. Almazán-Ruiz, J. Gómez, E.P. Rivero, O. Monroy, I. González, Hydrodynamic study of a novel membrane aerated biofilm reactor (MABR): Tracer experiments and CFD simulation, Chemical Engineering Science. 138 (2015) 324–332. https://doi.org/10.1016/j.ces.2015.08.004.
[52] W.P.M. Van Swaaij, J.C. Charpentier, J. Villermaux, Residence time distribution in the liquid phase of trickle flow in packed columns, Chemical Engineering Science. 24 (1969) 1083–1095. https://doi.org/10.1016/0009-2509(69)80080-1.
[53] S.F. Chung, C.Y. Wen, Longitudinal dispersion of liquid flowing through fixed and fluidized beds, AIChE Journal. 14 (1968) 857–866. https://doi.org/10.1002/aic.690140608.
[54] J.M.P.Q. Delgado, A critical review of dispersion in packed beds, Heat Mass Transfer. 42 (2006) 279–310. https://doi.org/10.1007/s00231-005-0019-0.
[55] M.-C. Yang, E.L. Cussler, Designing hollow-fiber contactors, AIChE J. 32 (1986) 1910–1916. https://doi.org/10.1002/aic.690321117.
[56] F. Séguret, Y. Racault, M. Sardin, Hydrodynamic behaviour of full scale trickling filters, Water Research. 34 (2000) 1551–1558. https://doi.org/10.1016/S0043-1354(99)00317-6.
[57] M. Hanhoun, L. Montastruc, C. Azzaro-Pantel, B. Biscans, M. Frèche, L. Pibouleau, Temperature impact assessment on struvite solubility product: A thermodynamic modeling approach, Chemical Engineering Journal. 167 (2011) 50–58. https://doi.org/10.1016/j.cej.2010.12.001.
[58] X. Liu, J. Wang, Impact of calcium on struvite crystallization in the wastewater and its competition with magnesium, Chemical Engineering Journal. 378 (2019) 122121. https://doi.org/10.1016/j.cej.2019.122121.
[59] W. Stumm, J.J. Morgan, Aquatic Chemistry: Chemical Equilibria and Rates in Natural Waters, John Wiley & Sons, 2012.
[60] M. Hanhoun, Analyse et modélisation de la précipitation de struvite : vers le traitement d'effluents aqueux industriels, PhD Thesis, University of Toulouse, 2011.
[61] V. Oliveira, C. Horta, C. Dias-Ferreira, Evaluation of a phosphorus fertiliser produced from anaerobically digested organic fraction of municipal solid waste, Journal of Cleaner Production. 238 (2019) 117911. https://doi.org/10.1016/j.jclepro.2019.117911.
[62] S. Hukari, L. Hermann, A. Nättorp, From wastewater to fertilisers — Technical overview and critical review of European legislation governing phosphorus recycling, Science of The Total Environment. 542 (2016) 1127–1135. https://doi.org/10.1016/j.scitotenv.2015.09.064.